THE EUROPEAN
PHYSICAL JOURNAL C

Check for updates

Regular Article - Experimental Physics

Measurement of the branching fraction of the $B^0 \to D_s^+ \pi^-$ decay

LHCb Collaboration⋆

CERN, 1211 Geneva 23, Switzerland

Abstract A branching fraction measurement of the $B^0 \to D_s^+ \pi^-$ decay is presented using proton–proton collision data collected with the LHCb experiment, corresponding to an integrated luminosity of $5.0\,\mathrm{fb}^{-1}$. The branching fraction is found to be $\mathcal{B}(B^0 \to D_s^+ \pi^-) = (19.4 \pm 1.8 \pm 1.3 \pm 1.2) \times 10^{-6}$, where the first uncertainty is statistical, the second systematic and the third is due to the uncertainty on the $B^0 \to D^- \pi^+$, $D_s^+ \to K^+ K^- \pi^+$ and $D^- \to K^+ \pi^- \pi^-$ branching fractions. This is the most precise single measurement of this quantity to date. As this decay proceeds through a single amplitude involving a $b \to u$ charged-current transition, the result provides information on non-factorisable strong interaction effects and the magnitude of the Cabibbo–Kobayashi–Maskawa matrix element V_{ub}. Additionally, the collision energy dependence of the hadronisation-fraction ratio f_s/f_d is measured through $\overline{B}_s^0 \to D_s^+ \pi^-$ and $B^0 \to D^- \pi^+$ decays.

1 Introduction

To test the Cabibbo–Kobayashi–Maskawa (CKM) sector of the Standard Model (SM), it is crucial to perform accurate measurements of the quark-mixing matrix elements. Any discrepancy among the numerous measurements of CKM matrix elements could reveal effects from new particles or forces beyond the SM. The knowledge of the magnitude of the matrix element V_{ub} governing the strength of $b \to u$ transitions is key in the consistency checks of the SM and its naturally motivated extensions [1,2].

The hadronic $B^0 \to D_s^+ \pi^-$ decay[1] proceeds in the SM through the $b \to u$ transition as shown in Fig. 1. Its branching fraction is proportional to $|V_{ub}|^2$,

$$\mathcal{B}(B^0 \to D_s^+ \pi^-) = \Phi |V_{ub}|^2 |V_{cs}|^2 |F(B^0 \to \pi^-)|^2 f_{D_s^+}^2 |a_{\mathrm{NF}}|^2, \quad (1)$$

where Φ is a phase-space factor, $F(B^0 \to \pi^-)$ is a form factor, $f_{D_s^+}$ is the D_s^+ decay constant, V_{cs} is the CKM matrix element representing $c \to s$ transitions, and $|a_{\mathrm{NF}}|$ encapsulates non-factorisable effects. The form factor and the decay constant can be obtained from light-cone sum rules [3,4] and lattice QCD calculations [5,6], and since $|V_{cs}|$ is known to be close to unity, the $B^0 \to D_s^+ \pi^-$ branching fraction can be used to probe the product $|V_{ub}||a_{\mathrm{NF}}|$. The assumption of factorisation is expected to hold, *i.e.* $|a_{\mathrm{NF}}|$ is close to unity, for B meson decays into a heavy and a light meson, where the W emission of the decay corresponds to the light meson and the spectator quark forms part of the heavy meson. This is not the case for the $B^0 \to D_s^+ \pi^-$ decay, as shown in Fig 1, and consequently $|a_{\mathrm{NF}}|$ may be significantly different from unity [7].

The measurement of the $B^0 \to D_s^+ \pi^-$ branching fraction can also be used to estimate the ratio of the amplitudes of the Cabibbo-suppressed $B^0 \to D^+ \pi^-$ and the Cabibbo-favoured $B^0 \to D^- \pi^+$ decays,

$$r_{D\pi} = \left| \frac{A(B^0 \to D^+ \pi^-)}{A(B^0 \to D^- \pi^+)} \right|, \quad (2)$$

which is necessary for the measurement of charge-parity (CP) asymmetries in $B^0 \to D^\mp \pi^\pm$ decays [8–13]. Assuming SU(3) flavour symmetry, Eq. (2) can be written as [14,15]

$$r_{D\pi} = \tan \theta_c \frac{f_{D^+}}{f_{D_s^+}} \sqrt{\frac{\mathcal{B}(B^0 \to D_s^+ \pi^-)}{\mathcal{B}(B^0 \to D^- \pi^+)}}, \quad (3)$$

where θ_c is the Cabibbo angle and f_{D^+} is the decay constant of the D^+ meson. SU(3) symmetry breaking is caused by different non-factorisable effects in in $B^0 \to D_s^+ \pi^-$ and $B^0 \to D^+ \pi^-$ decays.

---

[1] Inclusion of charge-conjugate modes is implied unless explicitly stated.
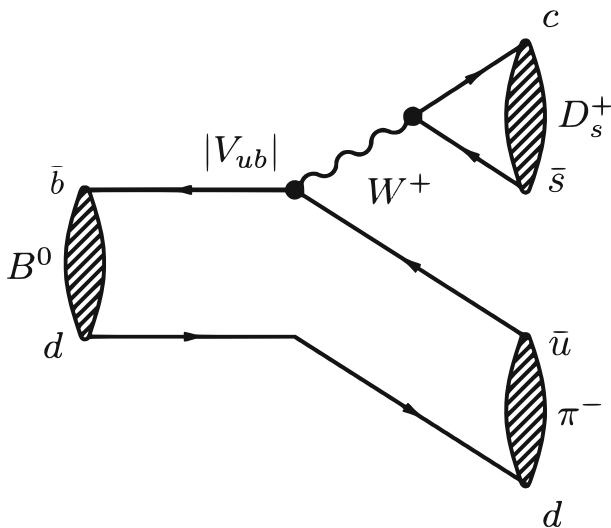
⋆ e-mail: jordy.butter@cern.ch

🍂 Springer

Fig. 1 Tree diagram of the $B^0 \to D_s^+ \pi^-$ decay, in which a B^0 meson decays through the weak interaction to a D_s^+ meson and a charged pion. This diagram represents the only (leading order) process contributing to this decay. Strong interaction between the D_s^+ meson and the pion lead to a non-factorisable contribution to the decay amplitude

This article presents measurements of $\mathcal{B}(B^0 \to D_s^+ \pi^-)$ and $r_{D\pi}$ using proton–proton (pp) collision data collected with the LHCb detector at centre-of-mass energies of 7, 8 and 13 TeV corresponding to an integrated luminosity of 5 fb^{-1}. The data samples recorded in the years 2011 and 2012 (2015 and 2016) at 7 and 8 (13) TeV will be referred to as Run 1 (Run 2). The $B^0 \to D_s^+ \pi^-$ branching ratio is measured relative to the $B^0 \to D^- \pi^+$ normalisation channel, which is well measured and experimentally similar to the $B^0 \to D_s^+ \pi^-$ decay. The $B^0 \to D_s^+ \pi^-$ ($B^0 \to D^- \pi^+$) candidates are reconstructed via the $D_s^+ \to K^+ K^- \pi^+$ ($D^- \to K^+ \pi^- \pi^-$) decay. The branching fraction of the $B^0 \to D_s^+ \pi^-$ decay is determined by

$$\mathcal{B}(B^0 \to D_s^+ \pi^-) = \mathcal{B}(B^0 \to D^- \pi^+) \frac{N_{B^0 \to D_s^+ \pi^-}}{N_{B^0 \to D^- \pi^+}} \frac{\epsilon_{B^0 \to D^- \pi^+}}{\epsilon_{B^0 \to D_s^+ \pi^-}}$$
$$\times \frac{\mathcal{B}(D^- \to K^+ \pi^- \pi^-)}{\mathcal{B}(D_s^+ \to K^+ K^- \pi^+)}, \qquad (4)$$

where N_X denotes the selected candidate yield and ϵ_X the related efficiency for the decay mode X. In this measurement, extended maximum-likelihood fits to unbinned invariant mass distributions are performed in order to obtain the yields, while the efficiencies are obtained from simulated events and using calibration data samples.

The relative production of B_s^0 and B^0 mesons, described by the ratio f_s/f_d where f_s and f_d are the B_s^0 and B^0 hadronisation fractions, is shown to slightly depend on the pp collision energy [16]. The efficiency-corrected yield ratio $\mathcal{R}$,

$$\mathcal{R} \equiv \frac{N_{\overline{B}_s^0 \to D_s^+ \pi^-}}{N_{B^0 \to D^- \pi^+}} \frac{\epsilon_{B^0 \to D^- \pi^+}}{\epsilon_{\overline{B}_s^0 \to D_s^+ \pi^-}} \propto \frac{f_s}{f_d}, \qquad (5)$$

is proportional to the relative production ratio and its dependence on the centre-of-mass energy is also reported here. This is measured using $\overline{B}_s^0 \to D_s^+ \pi^-$ and $B^0 \to D^- \pi^+$ decays. Accurate knowledge of f_s/f_d is a crucial input for every B_s^0 branching fraction measurement, *e.g.* $\mathcal{B}(B_s^0 \to \mu^+ \mu^-)$, since it dominates in most cases the systematic uncertainty [17]. Following the method described in Ref. [18], the value of f_s/f_d can be calculated as

$$\frac{f_s}{f_d} = 0.982 \frac{\tau_{B_d}}{\tau_{B_s}} \frac{\mathcal{R}}{\mathcal{N}_a \mathcal{N}_F \mathcal{N}_E} \frac{\mathcal{B}(D^- \to K^+ \pi^- \pi^-)}{\mathcal{B}(D_s^+ \to K^+ K^- \pi^+)}, \qquad (6)$$

where $\mathcal{R}$ is defined in Eq. (5), the numerical factor takes phase-space effects into account, $\mathcal{N}_a$ describes non-factorisable SU(3) breaking effects, $\mathcal{N}_F$ is the ratio of the form factors, $\mathcal{N}_E$ takes into account the contribution of the W-exchange diagram in the $B^0 \to D^- \pi^+$ decay, and τ_{B_d} (τ_{B_s}) is the B^0 (B_s^0) lifetime.

2 Detector and simulation

The LHCb detector [19,20] is a single-arm forward spectrometer covering the pseudorapidity range $2 < \eta < 5$, designed for the study of particles containing b or c quarks. The detector includes a high-precision tracking system consisting of a silicon-strip vertex detector surrounding the pp interaction region [21], a large-area silicon-strip detector located upstream of a dipole magnet with a bending power of about 4 Tm, and three stations of silicon-strip detectors and straw drift tubes [22,23] placed downstream of the magnet. The tracking system provides a measurement of the momentum, p, of charged particles with a relative uncertainty that varies from about 0.5% below 20 GeV/c to 1.0% at 200 GeV/c. The minimum distance of a track to a primary vertex (PV), the impact parameter (IP), is measured with a resolution of $(15+29/p_T)$ μm, where p_T is the component of the momentum transverse to the beam, in GeV/c. Different types of charged hadrons are distinguished using information from two ring-imaging Cherenkov (RICH) detectors [24]. Hadrons are identified by a calorimeter system consisting of scintillating-pad and preshower detectors, an electromagnetic and a hadronic calorimeter. Muons are identified by a system composed of alternating layers of iron and multiwire proportional chambers [25].

The online event selection is performed by a trigger [26], which consists of a hardware stage, based on information from the calorimeter and muon systems, followed by a software stage, which applies a full event reconstruction.

Simulation is required to calculate geometrical, reconstruction and selection efficiencies, and to determine shapes of invariant mass distributions. In the simulation, pp collisions are generated using PYTHIA [27] with a specific LHCb configuration [28]. Decays of unstable particles are described

by EvtGen [29], in which final-state radiation is generated using Photos [30]. The interaction of the generated particles with the detector, and its response, are implemented using the Geant4 toolkit [31,32] as described in Ref. [33].

3 Selection

The $B^0 \to D_s^+ \pi^-$ ($B^0 \to D^- \pi^+$) decays are reconstructed by forming a $D_s^+ \to K^+ K^- \pi^+$ ($D^- \to K^+ \pi^- \pi^-$) candidate and combining it with an additional pion of opposite charge, referred to as the companion. The same reconstruction and selection procedure is applied to the $\overline{B}_s^0 \to D_s^+ \pi^-$ decay. For the $B^0 \to D_s^+ \pi^-$ decay, the invariant mass of the $K^+ K^-$ pair is required to be within $20 \, \text{MeV}/c^2$ of the $\phi(1020)$ mass to select only the $D_s^+ \to \phi(1020) \pi^+$ decays, which significantly improves the signal-to-background ratio compared to other decays with a $K^+ K^- \pi^+$ combination in the final state. Selecting $D_s^+ \to \phi(1020) \pi^+$ decays has an efficiency of about 40%.

At the hardware trigger stage, events are required to have a muon with high p_T or a hadron, photon or electron with high transverse energy in the calorimeters. For hadrons, the transverse-energy threshold varied between 3 and 4 Ge V between 2011 and 2016. The software trigger requires a two-, three- or four-track secondary vertex with significant displacement from any primary pp interaction vertex (PV). At least one charged particle must have transverse momentum $p_T > 1.6 \, \text{GeV}/c$ and be inconsistent with originating from a PV. A multivariate algorithm [34] is used for the identification of secondary vertices consistent with the decay of a b hadron.

After the trigger selection, a preselection is applied to the reconstructed candidates to ensure good quality for the vertex of the b-hadron and c-hadron candidates comprising of tracks with large total and transverse momentum. Combinatorial background is suppressed using a gradient boosted decision tree (BDTG) algorithm [35,36], trained on Run 1 $\overline{B}_s^0 \to D_s^+ \pi^-$ data. A set of 15 variables is used to train the BDTG classifier, the ones with highest importance in the training being the transverse momentum of the companion pion, the radial flight distance of the $\overline{B}_s^0$ and of the D_s^+ candidates, the minimum transverse momentum of the D_s^+ decay products and the minimum χ_{IP}^2 of the companion and the $\overline{B}_s^0$ candidates, where χ_{IP}^2 is defined as the difference in the vertex-fit χ^2 of a given PV reconstructed with and without the particle under consideration. The correlation among the input variables has been studied and was found to be small. The BDTG classifier used in this measurement is described in Ref. [37].

To improve the B^0 and $\overline{B}_s^0$ invariant mass resolutions, the D_s^+ and D^- invariant masses are constrained to their known values [38]. All $D_s^+ \pi^-$ ($D^- \pi^+$) candidates are required

to have their invariant masses, $m(D_s^+ \pi^-)$ ($m(D^- \pi^+)$), within the range 5150–5800 (5000–5800) MeV/c^2 and the $K^+ K^- \pi^+$ ($K^+ \pi^- \pi^-$) invariant mass within 1930–2065 (1830–1920) MeV/c^2. The range of the $K^+ K^- \pi^+$ invariant mass includes a large upper sideband to model properly the combinatorial background shape, as described in Sect. 4.

To reduce the background due to misidentified final-state particles, particle identification (PID) information from the RICH detectors is used. The companion pion is required to pass a strict PID requirement to reduce the number of $\overset{(-)}{B_s^0} \to D_s^+ K^-$ ($B^0 \to D^- K^+$) decays where the kaon companion is misidentified as a pion. For $D_s^+ \to \phi(1020) \pi^+$ candidates, loose PID requirements are applied to both kaons and the pion, which imply a signal efficiency of about 96%. In the case of the pion, the PID requirement is used primarily to remove protons originating from the $\Lambda_c^+ \to \phi p$ decay. Further PID requirements are applied to veto $\Lambda_b^0 \to \Lambda_c^+ (\to p K^- \pi^+) \pi^-$ and $\overline{B}^0 \to D^+ (\to K^- \pi^+ \pi^+) \pi^-$ and $\overline{\Lambda}_b^0 \to \overline{\Lambda}_c^- (\to \overline{p} K^+ \pi^-) \pi^+$ and $B_s^0 \to D_s^- (\to K^- K^+ \pi^-) \pi^+$ events, which are misidentified as the final-state particles of $D_s^+ (\to K^+ K^- \pi^+) \pi^-$ and $D^- (\to K^+ \pi^- \pi^-) \pi^+$ decays, respectively. These vetoes are applied if candidates are consistent with the above mentioned decays when a mass hypothesis is changed. The PID requirements result in 75% efficiency for $B^0 \to D_s^+ \pi^-$ signal decays, which is dominated by the strict PID requirement on the companion pion, while the retention is about 9% for the $\overset{(-)}{B_s^0} \to D_s^+ K^-$ misidentified background contribution.

The event selection efficiencies are calculated from simulation with the exception of the efficiency of the PID requirements which is determined using calibration data samples.

4 Signal and background parametrisation

After the full event selection, unbinned maximum-likelihood fits are performed to obtain the yields of the signal $B^0 \to D_s^+ \pi^-$ and the normalisation $B^0 \to D^- \pi^+$ candidates. A two-dimensional fit to the $D_s^+ \pi^-$ and the $K^+ K^- \pi^+$ invariant mass distributions is performed to determine the $B^0 \to D_s^+ \pi^-$ signal yield, while the yield of the normalisation channel is obtained from a fit to the $D^- \pi^+$ invariant mass distribution. Due to the D_s^+ mass constraint, the correlation between $m(D_s^+ \pi^-)$ and $m(K^+ K^- \pi^+)$ is found to be small, thus the two variables are factorised in the fit model [39]. The two-dimensional fit is performed in order to constrain the combinatorial background (see further in this Section for details).

The $B^0 \to D_s^+ \pi^-$ decay is Cabibbo-suppressed and is therefore considerably less abundant than the Cabibbo-

favoured $\overline{B}^0_s \to D^+_s \pi^-$ decay, which produces the same final-state particles. The $m(D^+_s \pi^-)$ and $m(D^- \pi^+)$ shapes for $\overline{B}^0_s \to D^+_s \pi^-$ and $B^0 \to D^- \pi^+$ candidates, respectively, are described by the sum of a double-sided Hypatia function [40] and a Johnson S_U function [41]. The left tail of the $\overline{B}^0_s \to D^+_s \pi^-$ invariant mass distribution overlaps with the $B^0 \to D^+_s \pi^-$ signal peak and therefore special attention is given to the description of the lower mass range of the $\overline{B}^0_s \to D^+_s \pi^-$ peak, shaped by the combination of detector resolution and radiative effects. The $B^0 \to D^+_s \pi^-$ signal is described with the same model as the $\overline{B}^0_s \to D^+_s \pi^-$ decay, shifted by the known B^0–B^0_s mass difference [38]. The left tail of this distribution is described by two parameters, a_1 and n_1, which are found to be correlated and therefore the parameter n_1 is fixed to the value obtained from simulation, whereas a_1 is obtained from simulated $\overline{B}^0_s \to D^+_s \pi^-$ and $B^0 \to D^- \pi^+$ events, as well as from $B^0 \to D^- \pi^+$ data. In the invariant mass fit to $B^0 \to D^- \pi^+$ candidates the common mean of the double-sided Hypatia and the Johnson S_U functions, the widths and the left-tail parameter a_1 are left free in the fit, while this parameter is constrained in the $D^+_s \pi^-$ invariant mass distribution, as the background does not allow to determine the shape of the radiative tail reliably. All other parameters are fixed from simulation. In the $K^+ K^- \pi^+$ invariant mass fit a sum of two Crystal Ball functions with a common mean is used. The common mean and a scale factor for the widths are left free, while the other shape parameters are fixed from simulation.

The combinatorial background in $B^0 \to D^+_s \pi^-$ candidates is split in two components, referred to as random-D^+_s and true-D^+_s. The random-D^+_s combinatorial background consists of random combinations of tracks that do not peak in the $K^+ K^- \pi^+$ invariant mass, while the true-D^+_s combinatorial background consists of events with a true D^+_s meson, combined with a random companion track. The upper mass range of the $K^+ K^- \pi^+$ candidate sample is used to account accurately for the random-D^+_s component, modelled with a single exponential distribution, while the true-D^+_s background is described by the signal shape. In the $D^+_s \pi^-$ invariant mass fit, the random-D^+_s background is described by an exponential distribution and the true-D^+_s background is described by the sum of an exponential and a constant function. The exponential parameters are left free in both invariant mass fits.

The combinatorial background in the $m(D^- \pi^+)$ fit of the normalisation channel is described by the sum of an exponential and a constant function, with the relative weight of the two functions and exponential parameter left free.

Decays where one or more final-state particles are not reconstructed are referred to as partially reconstructed backgrounds. In the $D^+_s \pi^-$ and $D^- \pi^+$ invariant mass fits these background contributions are described by an upward-open parabola or a parabola exhibiting a maximum, whose ranges are defined by the kinematic endpoints of the decay, which are convolved with Gaussian resolution functions, and which are known to describe decays involving a missing neutral pion or a missing photon, as defined in Ref. [42]. In the fit to the $K^+ K^- \pi^+$ invariant mass, the partially reconstructed background contributions are described by the signal mass shape.

The $m(D^+_s \pi^-)$ fit requires two partially reconstructed background components from $\overline{B}^0_s \to D^{*+}_s (\to D^+_s \gamma/\pi^0) \pi^-$ and $\overline{B}^0_s \to D^+_s \rho^- (\to \pi^- \pi^0)$ decays. The fit model describing the $D^- \pi^+$ invariant mass accounts analogously for two partially reconstructed background contributions: $B^0 \to D^{*-} (\to D^- \pi^0) \pi^+$ and $B^0 \to D^- \rho^+ (\to \pi^+ \pi^0)$. In the case of the $\overline{B}^0_s \to D^{*+}_s \pi^-$ background the previously mentioned upward-open parabola together with a parabola exhibiting a maximum is used to parameterise the components with $D^{*+}_s \to D^+_s \gamma$ and $D^{*+}_s \to D^+_s \pi^0$ decays, respectively. The $\overline{B}^0_s \to D^+_s \rho^-$ background is described by the upward-open parabola, to take into account the missing neutral pion. The $B^0 \to D^{*-} \pi^+$ decay uses an upward-open parabola function and exhibits a double-peaked shape. Most parameters are obtained from simulated events and fixed, aside from the relevant invariant mass shifts and widths. For the $B^0 \to D^- \rho^+$ background a single upward-open parabola function is taken, with a floating width and a floating mass shift parameter that is shared with the $B^0 \to D^{*-} \pi^+$ contribution. The widths of the partially reconstructed background contributions in the $m(D^+_s \pi^-)$ fits are fixed to the values obtained from $B^0 \to D^- \pi^+$ candidates in data, corrected for differences between the $m(D^+_s \pi^-)$ and $m(D^- \pi^+)$ distributions, as obtained from simulation.

The $B^0 \to D^- \pi^+$ candidate sample is contaminated by the $B^0_s \to D^-_s \pi^+$, $\overline{\Lambda}^0_b \to \overline{\Lambda}^-_c \pi^+$ and $B^0 \to D^- K^+$ decays, resulting from the misidentification of one or two of the final-state particles. Analogously, the $\overline{B}^0_s \to D^+_s K^-$, $\Lambda^0_b \to \Lambda^+_c \pi^-$ and $\overline{B}^0 \to D^+ \pi^-$ decays are misidentified background contributions of the $B^0 \to D^+_s \pi^-$ candidate sample. Their shapes are determined from simulation using a non-parametric kernel estimation method [43]. The yields of the misidentified background contributions are estimated by using known branching fractions [38] and efficiencies that are determined from simulated background decays. Each yield of a misidentified background in the fit model is constrained to be close to its estimated value and is allowed to vary within the corresponding uncertainty.
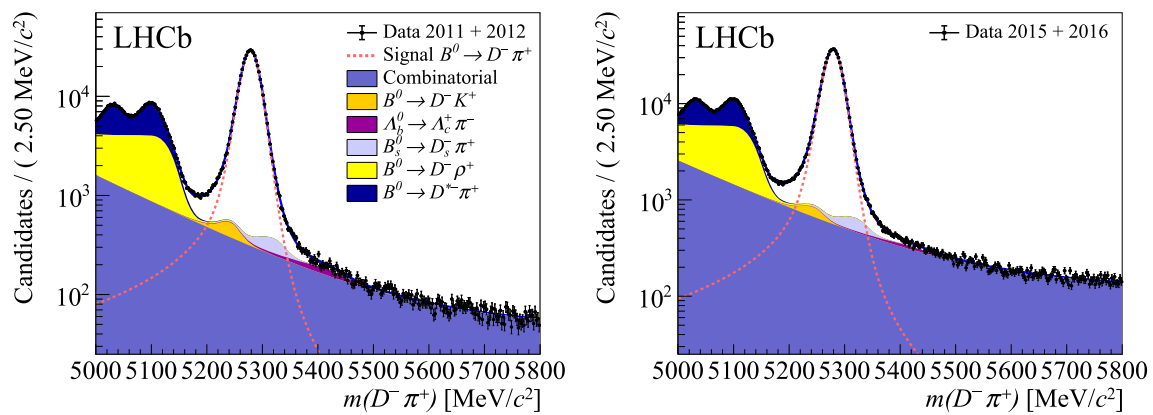
Fig. 2 The invariant mass distributions of normalisation $B^0 \to D^- \pi^+$ candidates, for (left) Run 1 and (right) Run 2 data samples. Overlaid are the fit projections along with the signal and background contributions

5 Signal yields

The $m(D^- \pi^+)$ data distributions, with overlaid fit projections for the total, the $B^0 \to D^- \pi^+$ signal and the background components, are shown in Fig. 2. The resulting signal yields are $(4.971 \pm 0.013) \times 10^5$ and $(6.294 \pm 0.016) \times 10^5$ for Run 1 and Run 2 samples, respectively. The fit results are also used to constrain the left tail of the signal shape and the widths of the partially reconstructed backgrounds to the invariant mass distribution of $B^0 \to D_s^+ \pi^-$ candidates.

The two-dimensional fit to $B^0 \to D_s^+ \pi^-$ candidates is performed in the $D_s^+ \pi^-$ and $K^+ K^- \pi^+$ invariant mass distributions. The $B^0 \to D_s^+ \pi^-$ branching fraction is determined using the yields of the signal and normalisation modes, their selection efficiencies and the known $B^0 \to D^- \pi^+$, $D^- \to K^+ \pi^- \pi^-$ and $D_s^+ \to K^+ K^- \pi^+$ branching fractions [38]. The two-dimensional fit is performed simultaneously for Run 1 and Run 2 data samples in which the $\mathcal{B}(B^0 \to D_s^+ \pi^-)$ and left-tail parameter are shared. The fit results in $B^0 \to D_s^+ \pi^-$ signal yields of $(8.9 \pm 0.8) \times 10^2$ and $(1.12 \pm 0.11) \times 10^3$ and $\overline{B}_s^0 \to D_s^+ \pi^-$ yields of $(3.370 \pm 0.023) \times 10^4$ and $(4.647 \pm 0.027) \times 10^4$ for Run 1 and Run 2 samples, respectively. Figure 3 shows the $D_s^+ \pi^-$ invariant mass distributions together with the fit projections and background contributions overlaid. Additionally, the invariant mass fits to $B^0 \to D^- \pi^+$ and $B^0 \to D_s^+ \pi^-$ candidates are performed simultaneously to 2011, 2012 and Run 2 data in order to study the collision energy dependence of f_s/f_d, as is described in Sect. 7.

6 Systematic uncertainties

Systematic uncertainties on the $\mathcal{B}(B^0 \to D_s^+ \pi^-)$ measurement arise from choices in the fit model and the determination of trigger, BDT and PID efficiencies. Many possible sources of systematic uncertainty cancel in the ratio of either the yields or the efficiencies of $B^0 \to D_s^+ \pi^-$ and $B^0 \to D^- \pi^+$

events. A summary of all the systematic uncertainties is shown in Table 1. The precision of the measurement relies mostly on the accurate modelling of the signal shape and of the partially reconstructed backgrounds.

The most critical aspect of the signal shape is the description of the left tail of the $\overline{B}_s^0 \to D_s^+ \pi^-$ signal, affecting the composition of signal and background around the B^0 mass. The shape of the left tail was determined from $B^0 \to D^- \pi^+$ candidates, taking into account differences between the final states, as obtained from simulation, and was Gaussian constrained in the fit. A systematic uncertainty is assigned for the assumption of the signal shape. This is done by repeating the signal fit with a different parametrisation, *i.e.* the sum of a double-sided Hypatia function and a Gaussian function, which leads to a systematic uncertainty of 5.1%. This parametrisation was found to be the only alternative parametrisation that satisfactorily described simulated signal candidates. Furthermore, a systematic uncertainty is assigned by fixing the mean of the $B^0 \to D_s^+ \pi^-$ signal shape to the result of the $B^0 \to D^- \pi^+$ fit, rather than shifting by the known B^0–B_s^0 mass difference. Moreover, the width of the $B^0 \to D_s^+ \pi^-$ signal shape is scaled by the ratio of the known B^0 and B_s^0 masses. The widths of the partially reconstructed backgrounds is varied by ± 1 MeV/c^2, in order to cover the differences between data and simulation as well as the differences between the $D_s^+ \pi^-$ and $D^- \pi^+$ invariant mass distributions. The resulting difference between the signal yields is assigned as a systematic uncertainty.

The simulated samples are corrected for an imperfect modelling of the response of the particle identification algorithms as a function of the kinematical properties of the particle, using samples of D^{*+} calibration data. A systematic uncertainty associated with the PID efficiency evaluation is assigned by varying the corrections within their uncertainties. Proton misidentification is the most difficult to control accurately from data calibration samples, as relatively little calibration data is available in the kinematic region that over-
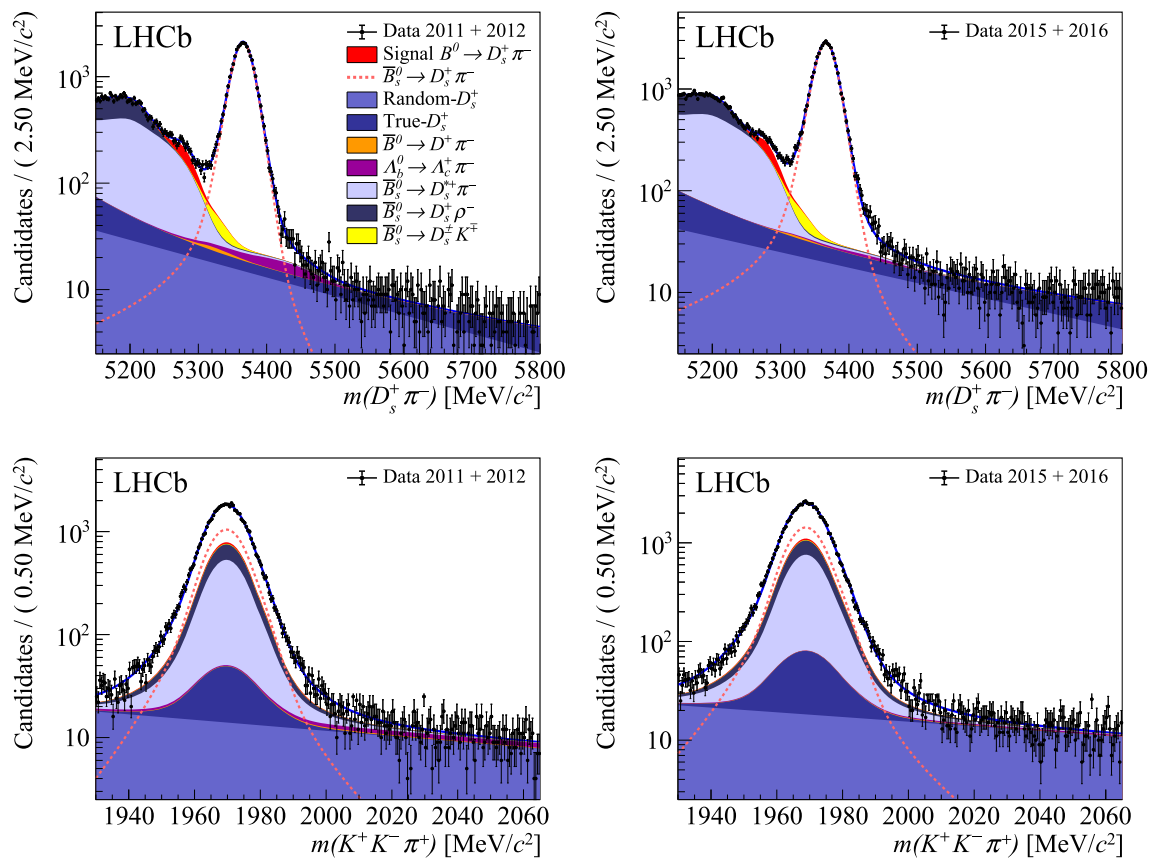
Fig. 3 The (top) $D_s^+\pi^-$ and (bottom) $K^+K^-\pi^+$ invariant mass distributions of signal $B^0 \to D_s^+\pi^-$ candidates, for (left) Run 1 and (right) Run 2 data samples. Overlaid are the fit projections along with the signal and background contributions

laps with the B decay products. In addition, the Cherenkov angles of photons emitted by protons and kaons are more similar than those of kaons and pions. Thus, a systematic uncertainty is estimated from the difference between the nominal signal yields and a fit where the misidentified background $\Lambda_b^0 \to \Lambda_c^+\pi^-$ decay yield is left free to vary.

The systematic uncertainty assigned to the hardware trigger efficiency takes into account a difference in detection efficiency between kaons and pions. This mostly cancels in the ratio of $B^0 \to D^-\pi^+$ and $B^0 \to D_s^+\pi^-$ efficiencies, but the difference of one final-state particle is sensitive to this detection asymmetry. Moreover, an uncertainty related to the reconstruction efficiency of charged particles is taken into account, which mainly arises from the uncertainty on the LHCb material and the different interaction cross-section of pions and kaons with the material [44]. Additionally, a systematic uncertainty is determined on the BDT efficiency due to the difference between simulation and data. This is determined by weighting all the BDT input variables in the simulated signal sample to the signal distributions in data, which are obtained using signal weights for each candidate using the *sPlot* technique [45].

Table 1 Relative systematic uncertainty σ on the $B^0 \to D_s^+\pi^-$ branching fraction measurement

Source	$\sigma(\mathcal{B}(B^0 \to D_s^+\pi^-))$ [%]
Fit model	
Signal shape parametrisation	5.1
$B^0 \to D_s^+\pi^-$ signal width	1.5
$B^0 \to D_s^+\pi^-$ mean	0.2
Partially reconstructed backgrounds	4.2
Misidentified backgrounds	0.6
Efficiencies	
Hardware trigger efficiency	0.3
Reconstruction efficiency	0.5
BDT efficiency	0.7
PID efficiency	1.1
Total	6.9

The systematic uncertainties on the collision energy dependence of the efficiency-corrected $\overline{B}_s^0 \to D_s^+\pi^-$ and $B^0 \to D^-\pi^+$ yield ratios are shown in Table 2. The sources of these systematic uncertainties are the same as for the

Table 2 Relative systematic uncertainty σ on the ratio of the efficiency-corrected $\overline{B}^0_s \to D^+_s \pi^-$ and $B^0 \to D^- \pi^+$ yield ratios. The ratios $\mathcal{R}_{13\,\text{TeV}}/\mathcal{R}_{7\,\text{TeV}}$ and $\mathcal{R}_{13\,\text{TeV}}/\mathcal{R}_{8\,\text{TeV}}$ are reported together as the difference of the systematic uncertainty for 7 and 8 TeV is negligible

Source	$\sigma\left(\dfrac{\mathcal{R}_{13\,\text{TeV}}}{\mathcal{R}_{7,8\,\text{TeV}}}\right)$[%]	$\sigma\left(\dfrac{\mathcal{R}_{8\,\text{TeV}}}{\mathcal{R}_{7\,\text{TeV}}}\right)$ [%]
Fit model		
Signal shape parametrisation	0.2	–
Misidentified backgrounds	0.2	–
Efficiencies		
Hardware trigger efficiency	0.4	0.4
BDT efficiency	1.1	1.3
PID efficiency	1.4	1.4
Total	1.9	2.0

Table 3 Results of $B^0 \to D^+_s \pi^-$ and $B^0 \to D^- \pi^+$ signal efficiencies and yields, as well as the branching fractions used as input for this measurement [38]

	Run 1	Run 2
$\epsilon_{B^0 \to D^+_s \pi^-}$ (%)	0.1412 ± 0.0010	0.1922 ± 0.0012
$\epsilon_{B^0 \to D^- \pi^+}$ (%)	0.3485 ± 0.0016	0.4536 ± 0.0016
$N_{B^0 \to D^- \pi^+}$	$(4.971 \pm 0.013) \times 10^5$	$(6.294 \pm 0.016) \times 10^5$
$N_{B^0 \to D^+_s \pi^-}$	$(8.9 \pm 0.8) \times 10^2$	$(1.12 \pm 0.11) \times 10^3$
$\mathcal{B}(B^0 \to D^- \pi^+)$	$(2.52 \pm 0.13) \times 10^{-3}$	
$\mathcal{B}(D^- \to K^+ \pi^- \pi^-)$	$(9.38 \pm 0.16) \times 10^{-2}$	
$\mathcal{B}(D^+_s \to K^+ K^- \pi^+)$	$(5.39 \pm 0.15) \times 10^{-2}$	

$B^0 \to D^+_s \pi^-$ branching fraction. Exceptions are the uncertainties on the $B^0 \to D^+_s \pi^-$ signal and the partially reconstructed backgrounds, which are found to be negligible, and the uncertainty on the charged-particle reconstruction efficiency, which cancels out in the double ratio of efficiencies.

7 Results

Table 3 gathers all measurements and inputs to determine the branching fraction according to Eq. (4). The branching fraction ratio of $B^0 \to D^+_s \pi^-$ and $B^0 \to D^- \pi^+$ decays is found to be

$$\frac{\mathcal{B}(B^0 \to D^+_s \pi^-)}{\mathcal{B}(B^0 \to D^- \pi^+)} = (7.7 \pm 0.7 \pm 0.5 \pm 0.3) \times 10^{-3},$$

where the first uncertainty is statistical, the second systematic and the third stems from knowledge of the $D^- \to K^+ \pi^- \pi^-$ and $D^-_s \to K^- K^+ \pi^-$ branching fractions.

Using the known value of $\mathcal{B}(B^0 \to D^- \pi^+)$ [38], the $B^0 \to D^+_s \pi^-$ branching fraction is found to be

$$\mathcal{B}(B^0 \to D^+_s \pi^-) = (19.4 \pm 1.8 \pm 1.3 \pm 1.2) \times 10^{-6},$$

where the first uncertainty is statistical, the second systematic and the third refers to the uncertainty due to the branching fractions listed in Table 3. This result represents the most precise single measurement of $\mathcal{B}(B^0 \to D^+_s \pi^-)$ to date.

The $B^0 \to D^+_s \pi^-$ branching fraction depends on both $|a_{\text{NF}}|$ and $|V_{ub}|$. Using the measurement of $\mathcal{B}(B^0 \to D^+_s \pi^-)$, the product

$$|V_{ub}||a_{\text{NF}}| = (3.14 \pm 0.20 \pm 0.25) \times 10^{-3}$$

is obtained, where the first uncertainty is from the $B^0 \to D^+_s \pi^-$ branching fraction measurement and the second from the CKM and QCD parameters. The form factor $F(B^0 \to \pi^-)|_{q^2 = m^2_{D^+_s}} = 0.327 \pm 0.025$ is obtained using light-cone sum rules [3,4] and lattice QCD calculations are used for the decay constant $f_{D^+_s} = 0.2499 \pm 0.0005$ Ge V [5,6]. A phase-space factor $\Phi = 296.2 \pm 0.8$ Ge V^{-2} is used in order to relate the branching fraction to $|V_{ub}||a_{\text{NF}}|$. Additionally, the CKM matrix element $|V_{cs}|$ is well measured and used as an input [38]. The determination of $|V_{ub}||a_{\text{NF}}|$ can be compared to the known inclusive and exclusive determinations of $|V_{ub}|$ to provide a constraint on the $|a_{\text{NF}}|$ parameter as displayed in Fig. 4.

The branching fraction ratio of $B^0 \to D^+_s \pi^-$ and $B^0 \to D^- \pi^+$ decays can be used to determine the parameter $r_{D\pi}$, as shown in Eq. (3). Inserting the measured branching fraction ratio $\mathcal{B}(B^0 \to D^+_s \pi^-)/\mathcal{B}(B^0 \to D^- \pi^+)$, the tangent of θ_c [38] and the fraction between the decay constants $f_{D^+_s}$ and f_{D^+} [5,6] into Eq. (3) gives

$$r_{D\pi} = 0.0163 \pm 0.0007 \pm 0.0007 \pm 0.0033,$$

where the first uncertainty is statistical, the second systematic and the third arises from possible non-factorisable SU(3)-breaking effects, estimated to be 20% according to Ref. [12]. SU(3)-breaking effects of about 20% are consistent with the measured $|a_{\text{NF}}|$ in this analysis, see Fig. 4.

Finally, the potential dependence of the hadronisation fraction f_s/f_d on collision energy is probed using the $B^0 \to D^- \pi^+$ and $\overline{B}^0_s \to D^+_s \pi^-$ signal yields obtained in the invariant mass fits, using Eq. (5). To determine these, the fit to Run 1 data is split based on collision energy into 2011 (7 TeV) and 2012 (8 TeV), sharing the shape parameters. The measured double ratios for the different collision energies are

$$\mathcal{R}_{13\,\text{TeV}}/\mathcal{R}_{7\,\text{TeV}} = 1.020 \pm 0.013 \pm 0.021,$$
$$\mathcal{R}_{13\,\text{TeV}}/\mathcal{R}_{8\,\text{TeV}} = 1.035 \pm 0.011 \pm 0.021,$$
$$\mathcal{R}_{8\,\text{TeV}}/\mathcal{R}_{7\,\text{TeV}} = 0.986 \pm 0.013 \pm 0.021,$$

where the first uncertainty is statistical and the second systematic. The average transverse momentum of the B meson after full event selection is found to be 10.4, 10.6 and 10.9 GeV/c for pp collision centre-of-mass energies of
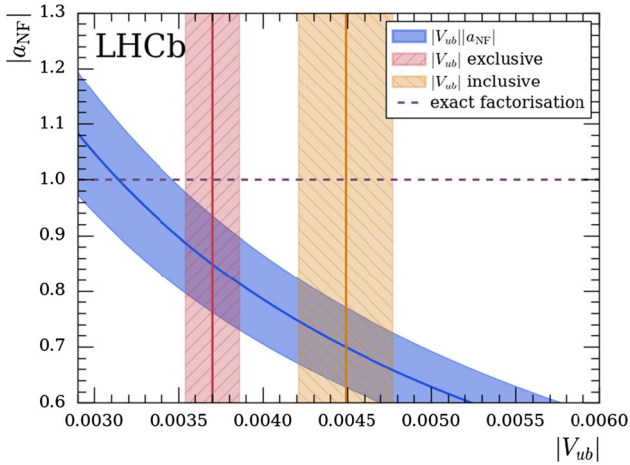
Fig. 4 Result of the determination of $|V_{ub}||a_{NF}|$. The blue line represents the result of this measurement, the vertical bands are the known exclusive and inclusive measurements of $|V_{ub}|$, which are $(3.70 \pm 0.16) \times 10^{-3}$ and $(4.49 \pm 0.28) \times 10^{-3}$, respectively [38]. The horizontal dashed line at $|a_{NF}| = 1.0$ represents exact factorisation. The error bands represent an uncertainty of one standard deviation

Fig. 5 Visualisation of the pp collision energy dependence of the efficiency-corrected yield ratio of $\overline{B}_s^0 \to D_s^+ \pi^-$ and $B^0 \to D^- \pi^+$ decays, which scales with f_s/f_d. The inner error bars indicate the statistical uncertainty only, whereas the outer indicate the uncorrelated, including statistical, uncertainties. The correlated systematic uncertainty is not shown. The red dotted line represents a linear fit through the three values of $\mathcal{R}$ with uncorrelated, including statistical, uncertainties

7 TeV, 8 TeV and 13 TeV, respectively. The separate values of $\mathcal{R}$ at the three collision energies are

$$\mathcal{R}_{7\,\text{TeV}} = 0.1631 \pm 0.0018 \pm 0.0025 \pm 0.0014,$$
$$\mathcal{R}_{8\,\text{TeV}} = 0.1609 \pm 0.0013 \pm 0.0024 \pm 0.0014,$$
$$\mathcal{R}_{13\,\text{TeV}} = 0.1665 \pm 0.0011 \pm 0.0023 \pm 0.0012,$$

where the first uncertainty is statistical and the following are the uncorrelated and correlated systematic uncertainties, respectively. The value of $\mathcal{R}$ at 7 TeV shows good agreement with the previous hadronic f_s/f_d measurement at 7 TeV, which was performed using $\overline{B}_s^0 \to D_s^+ \pi^-$, $B^0 \to D^- \pi^+$ and $B^0 \to D^- K^+$ decays [46]. A visualisation of the dependence of $\mathcal{R}$ on the centre-of-mass energy is given in Fig. 5. The resulting centre-of-mass energy dependence is obtained from a linear fit using the statistical and uncorrelated systematic uncertainties and is found to be $\mathcal{R} = 0.156(6) + 0.0008(6)\sqrt{s}$, where $\sqrt{s}$ is in TeV. The observed trend is in agreement with the LHCb measurement of the f_s/f_u dependence upon the pp collision energy [16]. The values for $\mathcal{R}$ will be used in a future work and can be used to obtain f_s/f_d by correcting $\mathcal{R}$ for the relative D branching fractions, the ratio of B lifetimes, the form factor ratio, the contribution from non-factorisable SU(3)-breaking effects and the contribution from the exchange diagram, as given by Eq. (6).
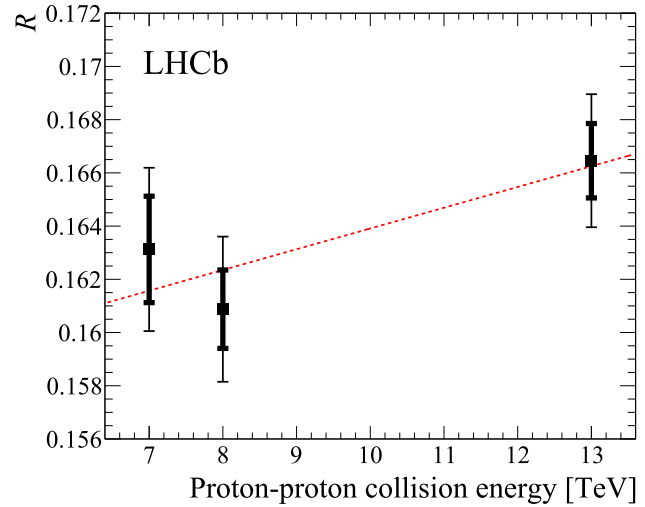
8 Summary

A branching fraction measurement of the $B^0 \to D_s^+ \pi^-$ decay is performed using pp collision data taken between 2011 and 2016, leading to

$$\mathcal{B}(B^0 \to D_s^+ \pi^-) = (19.4 \pm 1.8 \pm 1.3 \pm 1.2) \times 10^{-6},$$

where the first uncertainty is statistical, the second systematic and the third is due the branching fractions used as normalisation inputs. This is the most precise single measurement of $\mathcal{B}(B^0 \to D_s^+ \pi^-)$ to date, and is in agreement with the current world average [38]. Using this branching fraction, the product of $|V_{ub}|$ and the non-factorisation constant $|a_{NF}|$ is determined to be

$$|V_{ub}||a_{NF}| = (3.14 \pm 0.20 \pm 0.25) \times 10^{-3}.$$

Comparison with independently measured values of V_{ub} [38] indicate that $|a_{NF}|$ may deviate from unity by around 20%, indicating significant non-factorisable corrections.

The measurement of the ratio of the $B^0 \to D_s^+ \pi^-$ and $B^0 \to D^- \pi^+$ branching fractions is used to determine the $r_{D\pi}$ parameter,

$$r_{D\pi} = 0.0163 \pm 0.0007 \pm 0.0007 \pm 0.0033,$$

where the first uncertainty is statistical, the second systematic and the third arises from possible non-factorisable SU(3)-breaking effects, estimated to be 20% [12]. Knowledge of this parameter is essential to interpret the CP asymmetries in $B^0 \to D^{\mp} \pi^{\pm}$ decays.

Finally, the efficiency-corrected yield ratio of $\overline{B}^0_s \to D^+_s \pi^-$ and $B^0 \to D^- \pi^+$ decays, $\mathcal{R}$, is used to probe the collision energy dependence of the hadronisation fraction f_s/f_d.

Data Availability Statement This manuscript has no associated data or the data will not be deposited. [Authors' comment: All LHCb scientific output is published in journals, with preliminary results made available in Conference Reports. All are Open Access, without restriction on use beyond the standard conditions agreed by CERN. Data associated to the plots in this publication as well as in supplementary materials are made available on the CERN document server at https://cds.cern.ch/record/2742603. This information is taken from the LHCb External Data Access Policy which can be downloaded at http://opendata.cern.ch/record/410]

References

1. CKMfitter Group, J. Charles, et al., Current status of the standard model CKM fit and constraints on $\Delta F = 2$ new physics. Phys. Rev. D **91**, 073007 (2015). arXiv:1501.05013, updated results and plots available at http://www.ckmfitter.in2p3.fr/

2. UTfit Collaboration, M. Bona, et al., The unitarity triangle fit in the standard model and hadronic parameters from lattice QCD: a reappraisal after the measurements of Δm_s and $BR(B \to \tau \nu_\tau)$. JHEP **10**, 081 (2006). arXiv:hep-ph/0606167, updated results and plots available at http://www.utfit.org/

3. P. Ball, R. Zwicky, New results on $B \to \pi, K, \eta$ decay form factors from light-cone sum rules. Phys. Rev. D **71**, 014015 (2005). arXiv:hep-ph/0406232

4. P. Ball, $|V_{ub}|$ from UTangles and $B^0 \to \pi^- \ell^+ \nu$. Phys. Lett. B **644**, 38 (2007). arXiv:hep-ph/0611108

5. A. Bazavov et al., B- and D-meson leptonic decay constants from four-flavor lattice QCD. Phys. Rev. D **98**, 074512 (2018). arXiv:1712.09262

6. N. Carrasco et al., Leptonic decay constants f_K, f_D, and f_{D_s} with $N_f = 2+1+1$ twisted-mass lattice QCD. Phys. Rev. D **91**, 054507 (2015). arXiv:1411.7908

7. M. Beneke, G. Buchalla, M. Neubert, C.T. Sachrajda, QCD factorization for exclusive, nonleptonic B meson decays: general arguments and the case of heavy light final states. Nucl. Phys. B **591**, 313 (2000). arXiv:hep-ph/0006124

8. BaBar Collaboration, B. Aubert, et al., Measurement of time-dependent CP-violating asymmetries and constraints on $\sin(2\beta + \gamma)$ with partial reconstruction of $B \to D^{*\mp} \pi^\pm$ decays. Phys. Rev. D **71**, 112003 (2005). arXiv:hep-ex/0504035

9. BaBar Collaboration, B. Aubert, et al., Measurement of time-dependent CP asymmetries in $B^0 \to D^{(*)\pm} \pi^\mp$ and $B^0 \to D^\pm \rho^\mp$ decays. Phys. Rev. D **73**, 111101 (2006). arXiv:hep-ex/0602049

10. Belle Collaboration, F.J. Ronga, et al., Measurements of CP violation in $B^0 \to D^{*-} \pi^+$ and $B^0 \to D^- \pi^+$ decays. Phys. Rev. D **73**, 092003 (2006). arXiv:hep-ex/0604013

11. Belle Collaboration, S. Bahinipati, et al., Measurements of time-dependent CP asymmetries in $B \to D^{*\mp} \pi^\pm$ decays using a partial reconstruction technique. Phys. Rev. D **84**, 021101 (2011). arXiv:1102.0888

12. K. De Bruyn et al., Exploring $B_s \to D_s^{(*)\pm} K^\mp$ decays in the presence of a sizable width difference $\Delta\Gamma_s$. Nucl. Phys. B **868**, 351 (2013). arXiv:1208.6463

13. LHCb Collaboration, R. Aaij, et al., Measurement of CP violation in $B^0 \to D^\pm \pi^\mp$ decays. JHEP **06**, 084 (2018). arXiv:1805.03448

14. BaBar Collaboration, B. Aubert, et al., Measurement of the branching fractions of the rare decays $B^0 \to D_s^{(*)+} \pi^-$, $B^0 \to D_s^{(*)+} \rho^-$, and $B^0 \to D_s^{(*)-} K^{(*)+}$. Phys. Rev. D **78**, 032005 (2008). arXiv:0803.4296

15. Belle Collaboration, A. Das, et al., Measurements of branching fractions for $B^0 \to D_s^+ \pi^- \nu$ and $\bar{B}^0 \to D_s^+ K^-$. Phys. Rev. D **82**, 051103 (2010). arXiv:1007.4619

16. LHCb Collaboration, R. Aaij, et al., Measurement of f_s/f_u variation with proton-proton collision energy and B-meson kinematics. Phys. Rev. Lett. **124**, 122002 (2020). arXiv:1910.09934

17. LHCb Collaboration, R. Aaij, et al., Measurement of the $B_s^0 \to \mu^+ \mu^-$ branching fraction and effective lifetime and search for $B^0 \to \mu^+ \mu^-$ decays. Phys. Rev. Lett. **118**, 191801 (2017). arXiv:1703.05747

18. R. Fleischer, N. Serra, N. Tuning, Tests of factorization and SU(3) relations in B decays into heavy-light final states. Phys. Rev. D **83**, 014017 (2011). arXiv:1012.2784

19. LHCb Collaboration, A.A. Alves Jr., et al., The LHCb detector at the LHC. JINST **3**, S08005 (2008)

20. LHCb Collaboration, R. Aaij, et al., LHCb detector performance. Int. J. Mod. Phys. A **30**, 1530022 (2015). arXiv:1412.6352

21. R. Aaij et al., Performance of the LHCb Vertex Locator. JINST **9**, P09007 (2014). arXiv:1405.7808

22. R. Arink et al., Performance of the LHCb Outer Tracker. JINST **9**, P01002 (2014). arXiv:1311.3893

23. P. d'Argent et al., Improved performance of the LHCb Outer Tracker in LHC Run 2. JINST **12**, P11016 (2017). arXiv:1708.00819

24. M. Adinolfi et al., Performance of the LHCb RICH detector at the LHC. Eur. Phys. J. C **73**, 2431 (2013). arXiv:1211.6759

25. A.A. Alves Jr. et al., Performance of the LHCb muon system. JINST **8**, P02022 (2013). arXiv:1211.1346

26. R. Aaij et al., The LHCb trigger and its performance in 2011. JINST **8**, P04022 (2013). arXiv:1211.3055

27. T. Sjöstrand, S. Mrenna, P. Skands, A brief introduction to PYTHIA 8.1. Comput. Phys. Commun. **178**, 852 (2008). arXiv:0710.3820

28. I. Belyaev et al., Handling of the generation of primary events in Gauss, the LHCb simulation framework. J. Phys. Conf. Ser. **331**, 032047 (2011)

29. D.J. Lange, The EvtGen particle decay simulation package. Nucl. Instrum. Methods A **462**, 152 (2001)

30. P. Golonka, Z. Was, PHOTOS Monte Carlo: a precision tool for QED corrections in Z and W decays. Eur. Phys. J. C **45**, 97 (2006). arXiv:hep-ph/0506026

31. Geant4 Collaboration, J. Allison, et al., Geant4 developments and applications. IEEE Trans. Nucl. Sci. **53**, 270 (2006)

32. Geant4 Collaboration, S. Agostinelli, et al., Geant4: a simulation toolkit. Nucl. Instrum. Methods A **506**, 250 (2003)

33. M. Clemencic et al., The LHCb simulation application, Gauss: Design, evolution and experience. J. Phys. Conf. Ser. **331**, 032023 (2011). arXiv:1210.6861

34. V.V. Gligorov, M. Williams, Efficient, reliable and fast high-level triggering using a bonsai boosted decision tree. JINST **8**, P02013 (2013). arXiv:1210.6861

35. L. Breiman, J.H. Friedman, R.A. Olshen, C.J. Stone, *Classification and Regression Trees* (Wadsworth international group, Belmont, 1984)

36. B.P. Roe et al., Boosted decision trees, an alternative to artificial neural networks. Nucl. Instrum. Methods **A543**, 577 (2005). arXiv:physics/0408124

37. U.P. Eitschberger, Flavour-tagged measurement of CP observables in $B_s^0 \to D_s^{\mp} K^{\pm}$ decays with the LHCb experiment. Ph.D. thesis, Tech. U., Dortmund (main) (2018). https://doi.org/10.17877/DE290R-18881

38. Particle Data Group, P.A. Zyla, et al., Review of particle physics. Prog. Theor. Exp. Phys. **2020**, 083C01 (2020)

39. LHCb Collaboration, R. Aaij, et al., Measurement of CP asymmetry in $B_s^0 \to D_s^{\mp} K^{\pm}$ decays. JHEP **03**, 059 (2018). arXiv:1712.07428

40. D. Martínez Santos, F. Dupertuis, Mass distributions marginalized over per-event errors. Nucl. Instrum. Methods A **764**, 150 (2014). arXiv:1312.5000

41. N.L. Johnson, Systems of frequency curves generated by methods of translation. Biometrika **36**, 149 (1949)

42. LHCb Collaboration, R. Aaij, et al., Measurement of CP observables in $B^{\pm} \to D^{(*)} K^{\pm}$ and $B^{\pm} \to D^{(*)} \pi^{\pm}$ decays. Phys. Lett. B **777**, 16 (2018). arXiv:1708.06370

43. K.S. Cranmer, Kernel estimation in high-energy physics. Comput. Phys. Commun. **136**, 198 (2001). arXiv:hep-ex/0011057

44. LHCb Collaboration, R. Aaij, et al., Measurement of the branching fraction and CP asymmetry in $B^+ \to J/\pi \rho^+$ decays. Eur. Phys. J. C **79**, 537 (2019). arXiv:1812.07041

45. M. Pivk, F.R. Le Diberder, sPlot: a statistical tool to unfold data distributions. Nucl. Instrum. Methods A **555**, 356 (2005). arXiv:physics/0402083

46. LHCb Collaboration, R. Aaij, et al., Measurement of the fragmentation fraction ratio f_s/f_d and its dependence on B meson kinematics. JHEP **04**, 001 (2013). arXiv:1301.5286

LHCb Collaboration

R. Aaij[32], C. Abellán Beteta[50], T. Ackernley[60], B. Adeva[46], M. Adinolfi[54], H. Afsharnia[9], C. A. Aidala[85], S. Aiola[25], Z. Ajaltouni[9], S. Akar[65], J. Albrecht[15], F. Alessio[48], M. Alexander[59], A. Alfonso Albero[45], Z. Aliouche[62], G. Alkhazov[38], P. Alvarez Cartelle[55], S. Amato[2], Y. Amhis[11], L. An[48], L. Anderlini[22], A. Andreianov[38], M. Andreotti[21], F. Archilli[17], A. Artamonov[44], M. Artuso[68], K. Arzymatov[42], E. Aslanides[10], M. Atzeni[50], B. Audurier[12], S. Bachmann[17], M. Bachmayer[49], J. J. Back[56], S. Baker[61], P. Baladron Rodriguez[46], V. Balagura[12], W. Baldini[21], J. Baptista Leite[1], R. J. Barlow[62], S. Barsuk[11], W. Barter[61], M. Bartolini[24,g], F. Baryshnikov[82], J. M. Basels[14], G. Bassi[29], B. Batsukh[68], A. Battig[15], A. Bay[49], M. Becker[15], F. Bedeschi[29], I. Bediaga[1], A. Beiter[68], V. Belavin[42], S. Belin[27], V. Bellee[49], K. Belous[44], I. Belov[40], I. Belyaev[41], G. Bencivenni[23], E. Ben-Haim[13], A. Berezhnoy[40], R. Bernet[50], D. Berninghoff[17], H. C. Bernstein[68], C. Bertella[48], A. Bertolin[28], C. Betancourt[50], F. Betti[20,c], Ia. Bezshyiko[50], S. Bhasin[54], J. Bhom[35], L. Bian[73], M. S. Bieker[15], S. Bifani[53], P. Billoir[13], M. Birch[61], F. C. R. Bishop[55], A. Bizzeti[22,j], M. Bjørn[63], M. P. Blago[48], T. Blake[56], F. Blanc[49], S. Blusk[68], D. Bobulska[59], J. A. Boelhauve[15], O. Boente Garcia[46], T. Boettcher[64], A. Boldyrev[81], A. Bondar[43], N. Bondar[38], S. Borghi[62], M. Borisyak[42], M. Borsato[17], J. T. Borsuk[35], S. A. Bouchiba[49], T. J. V. Bowcock[60], A. Boyer[48], C. Bozzi[21], M. J. Bradley[61], S. Braun[66], A. Brea Rodriguez[46], M. Brodski[48], J. Brodzicka[35], A. Brossa Gonzalo[56], D. Brundu[27], A. Buonaura[50], C. Burr[48], A. Bursche[27], A. Butkevich[39], J. S. Butter[32] , J. Buytaert[48], W. Byczynski[48], S. Cadeddu[27], H. Cai[73], R. Calabrese[21,e], L. Calefice[13,15], L. Calero Diaz[23], S. Cali[23], R. Calladine[53], M. Calvi[26,i], M. Calvo Gomez[84], P. Camargo Magalhaes[54], A. Camboni[45,84], P. Campana[23], A. F. Campoverde Quezada[6], S. Capelli[26,i], L. Capriotti[20,c], A. Carbone[20,c], G. Carboni[31], R. Cardinale[24,g], A. Cardini[27], I. Carli[4], P. Carniti[26,i], K. Carvalho Akiba[32], A. Casais Vidal[46], G. Casse[60], M. Cattaneo[48], G. Cavallero[48], S. Celani[49], J. Cerasoli[10], A. J. Chadwick[60], M. G. Chapman[54], M. Charles[13], Ph. Charpentier[48], G. Chatzikonstantinidis[53], C. A. Chavez Barajas[60], M. Chefdeville[8], C. Chen[3], S. Chen[27], A. Chernov[35], S.-G. Chitic[48], V. Chobanova[46], S. Cholak[49], M. Chrzaszcz[35], A. Chubykin[38], V. Chulikov[38], P. Ciambrone[23], M. F. Cicala[56], X. Cid Vidal[46], G. Ciezarek[48], P. E. L. Clarke[58], M. Clemencic[48], H. V. Cliff[55], J. Closier[48], J. L. Cobbledick[62], V. Coco[48], J. A. B. Coelho[11], J. Cogan[10], E. Cogneras[9], L. Cojocariu[37], P. Collins[48], T. Colombo[48], L. Congedo[19,b], A. Contu[27], N. Cooke[53], G. Coombs[59], G. Corti[48], C. M. Costa Sobral[56], B. Couturier[48], D. C. Craik[64], J. Crkovská[67], M. Cruz Torres[1], R. Currie[58], C. L. Da Silva[67], E. Dall'Occo[15], J. Dalseno[46], C. D'Ambrosio[48], A. Danilina[41], P. d'Argent[48], A. Davis[62], O. De Aguiar Francisco[62], K. De Bruyn[78], S. De Capua[62], M. De Cian[49], J. M. De Miranda[1], L. De Paula[2], M. De Serio[19,b], D. De Simone[50], P. De Simone[23], J. A. de Vries[79], C. T. Dean[67], D. Decamp[8], L. Del Buono[13], B. Delaney[55], H.-P. Dembinski[15], A. Dendek[34], V. Denysenko[50], D. Derkach[81], O. Deschamps[9], F. Desse[11], F. Dettori[27,d], B. Dey[73], P. Di Nezza[23], S. Didenko[82], L. Dieste Maronas[46], H. Dijkstra[48], V. Dobishuk[52], A. M. Donohoe[18], F. Dordei[27], A. C. dos Reis[1], L. Douglas[59], A. Dovbnya[51], A. G. Downes[8], K. Dreimanis[60], M. W. Dudek[35], L. Dufour[48], V. Duk[77], P. Durante[48], J. M. Durham[67], D. Dutta[62], M. Dziewiecki[17], A. Dziurda[35], A. Dzyuba[38], S. Easo[57], U. Egede[69], V. Egorychev[41], S. Eidelman[43,u], S. Eisenhardt[58], S. Ek-In[49], L. Eklund[59,v], S. Ely[68], A. Ene[37], E. Epple[67], S. Escher[14], J. Eschle[50], S. Esen[32], T. Evans[48], A. Falabella[20], J. Fan[3], Y. Fan[6], B. Fang[73], N. Farley[53], S. Farry[60], D. Fazzini[26,i], P. Fedin[41], M. Féo[48], P. Fernandez Declara[48], A. Fernandez Prieto[46], J. M. Fernandez-tenllado Arribas[45], F. Ferrari[20,c], L. Ferreira Lopes[49], F. Ferreira Rodrigues[2], S. Ferreres Sole[32], M. Ferrillo[50], M. Ferro-Luzzi[48], S. Filippov[39], R. A. Fini[19], M. Fiorini[21,e], M. Firlej[34], K. M. Fischer[63], C. Fitzpatrick[62], T. Fiutowski[34], F. Fleuret[12], M. Fontana[13], F. Fontanelli[24,g], R. Forty[48], V. Franco Lima[60], M. Franco Sevilla[66], M. Frank[48], E. Franzoso[21], G. Frau[17], C. Frei[48], D. A. Friday[59], J. Fu[25], Q. Fuehring[15], W. Funk[48], E. Gabriel[32], T. Gaintseva[42], A. Gallas Torreira[46], D. Galli[20,c], S. Gambetta[48,58], Y. Gan[3], M. Gandelman[2], P. Gandini[25], Y. Gao[5], M. Garau[27], L. M. Garcia Martin[56], P. Garcia Moreno[45], J. García Pardiñas[26], B. Garcia Plana[46], F. A. Garcia Rosales[12], L. Garrido[45], C. Gaspar[48], R. E. Geertsema[32], D. Gerick[17], L. L. Gerken[15], E. Gersabeck[62], M. Gersabeck[62], T. Gershon[56], D. Gerstel[10], Ph. Ghez[8], V. Gibson[55], M. Giovannetti[23,o], A. Gioventù[46], P. Gironella Gironell[45], L. Giubega[37], C. Giugliano[21,e,48], K. Gizdov[58], E. L. Gkougkousis[48], V. V. Gligorov[13], C. Göbel[70], E. Golobardes[84], D. Golubkov[41], A. Golutvin[61,82], A. Gomes[1,a], S. Gomez Fernandez[45], F. Goncalves Abrantes[70], M. Goncerz[35], G. Gong[3], P. Gorbounov[41], I. V. Gorelov[40], C. Gotti[26,i], E. Govorkova[48], J. P. Grabowski[17], R. Graciani Diaz[45], T. Grammatico[13], L. A. Granado Cardoso[48], E. Graugés[45], E. Graverini[49], G. Graziani[22], A. Grecu[37], L. M. Greeven[32], P. Griffith[21,e], L. Grillo[62], S. Gromov[82], B. R. Gruberg Cazon[63], C. Gu[3], M. Guarise[21], P. A. Günther[17], E. Gushchin[39], A. Guth[14], Y. Guz[44,48], T. Gys[48], T. Hadavizadeh[69], G. Haefeli[49], C. Haen[48], J. Haimberger[48], T. Halewood-leagas[60], P. M. Hamilton[66], Q. Han[7], X. Han[17], T. H. Hancock[63], S. Hansmann-Menzemer[17], N. Harnew[63], T. Harrison[60], C. Hasse[48], M. Hatch[48], J. He[6], M. Hecker[61], K. Heijhoff[32], K. Heinicke[15], A. M. Hennequin[48], K. Hennessy[60], L. Henry[25,47], J. Heuel[14], A. Hicheur[2], D. Hill[49], M. Hilton[62], S. E. Hollitt[15], J. Hu[72], J. Hu[17], W. Hu[7], W. Huang[6], X. Huang[73], W. Hulsbergen[32], R. J. Hunter[56],

M. Hushchyn[81], D. Hutchcroft[60], D. Hynds[32], P. Ibis[15], M. Idzik[34], D. Ilin[38], P. Ilten[65], A. Inglessi[38], A. Ishteev[82], K. Ivshin[38], R. Jacobsson[48], S. Jakobsen[48], E. Jans[32], B. K. Jashal[47], A. Jawahery[66], V. Jevtic[15], M. Jezabek[35], F. Jiang[3], M. John[63], D. Johnson[48], C. R. Jones[55], T. P. Jones[56], B. Jost[48], N. Jurik[48], S. Kandybei[51], Y. Kang[3], M. Karacson[48], N. Kazeev[81], F. Keizer[48,55], M. Kenzie[56], T. Ketel[33], B. Khanji[15], A. Kharisova[83], S. Kholodenko[44], K. E. Kim[68], T. Kirn[14], V. S. Kirsebom[49], O. Kitouni[64], S. Klaver[32], K. Klimaszewski[36], S. Koliiev[52], A. Kondybayeva[82], A. Konoplyannikov[41], P. Kopciewicz[34], R. Kopecna[17], P. Koppenburg[32], M. Korolev[40], I. Kostiuk[32,52], O. Kot[52], S. Kotriakhova[30,38], P. Kravchenko[38], L. Kravchuk[39], R. D. Krawczyk[48], M. Kreps[56], F. Kress[61], S. Kretzschmar[14], P. Krokovny[43,u], W. Krupa[34], W. Krzemien[36], W. Kucewicz[35,s], M. Kucharczyk[35], V. Kudryavtsev[43,u], H. S. Kuindersma[32], G. J. Kunde[67], T. Kvaratskheliya[41], D. Lacarrere[48], G. Lafferty[62], A. Lai[27], A. Lampis[27], D. Lancierini[50], J. J. Lane[62], R. Lane[54], G. Lanfranchi[23], C. Langenbruch[14], J. Langer[15], O. Lantwin[50,82], T. Latham[56], F. Lazzari[29,p], R. Le Gac[10], S. H. Lee[85], R. Lefèvre[9], A. Leflat[40], S. Legotin[82], O. Leroy[10], T. Lesiak[35], B. Leverington[17], H. Li[72], L. Li[63], P. Li[17], Y. Li[4], Y. Li[4], Z. Li[68], X. Liang[68], T. Lin[61], R. Lindner[48], V. Lisovskyi[15], R. Litvinov[27], G. Liu[72], H. Liu[6], S. Liu[4], X. Liu[3], A. Loi[27], J. Lomba Castro[46], I. Longstaff[59], J. H. Lopes[2], G. Loustau[50], G. H. Lovell[55], Y. Lu[4], D. Lucchesi[28,k], S. Luchuk[39], M. Lucio Martinez[32], V. Lukashenko[32], Y. Luo[3], A. Lupato[62], E. Luppi[21,e], O. Lupton[56], A. Lusiani[29,l], X. Lyu[6], L. Ma[4], S. Maccolini[20,c], F. Machefert[11], F. Maciuc[37], V. Macko[49], P. Mackowiak[15], S. Maddrell-Mander[54], O. Madejczyk[34], L. R. Madhan Mohan[54], O. Maev[38], A. Maevskiy[81], D. Maisuzenko[38], M. W. Majewski[34], S. Malde[63], B. Malecki[48], A. Malinin[80], T. Maltsev[43,u], H. Malygina[17], G. Manca[27,d], G. Mancinelli[10], R. Manera Escalero[45], D. Manuzzi[20,c], D. Marangotto[25,h], J. Maratas[9,r], J. F. Marchand[8], U. Marconi[20], S. Mariani[22,f,48], C. Marin Benito[11], M. Marinangeli[49], P. Marino[49,l], J. Marks[17], P. J. Marshall[60], G. Martellotti[30], L. Martinazzoli[48,i], M. Martinelli[26,i], D. Martinez Santos[46], F. Martinez Vidal[47], A. Massafferri[1], M. Materok[14], R. Matev[48], A. Mathad[50], Z. Mathe[48], V. Matiunin[41], C. Matteuzzi[26], K. R. Mattioli[85], A. Mauri[32], E. Maurice[12], J. Mauricio[45], M. Mazurek[36], M. McCann[61], L. Mcconnell[18], T. H. Mcgrath[62], A. McNab[62], R. McNulty[18], J. V. Mead[60], B. Meadows[65], C. Meaux[10], G. Meier[15], N. Meinert[76], D. Melnychuk[36], S. Meloni[26,i], M. Merk[32,79], A. Merli[25], L. Meyer Garcia[2], M. Mikhasenko[48], D. A. Milanes[74], E. Millard[56], M. Milovanovic[48], M.-N. Minard[8], L. Minzoni[21,e], S. E. Mitchell[58], B. Mitreska[62], D. S. Mitzel[48], A. Mödden[15], R. A. Mohammed[63], R. D. Moise[61], T. Mombächer[15], I. A. Monroy[74], S. Monteil[9], M. Morandin[28], G. Morello[23], M. J. Morello[29,l], J. Moron[34], A. B. Morris[75], A. G. Morris[56], R. Mountain[68], H. Mu[3], F. Muheim[58], M. Mukherjee[7], M. Mulder[48], D. Müller[48], K. Müller[50], C. H. Murphy[63], D. Murray[62], P. Muzzetto[27,48], P. Naik[54], T. Nakada[49], R. Nandakumar[57], T. Nanut[49], I. Nasteva[2], M. Needham[58], I. Neri[21,e], N. Neri[25,h], S. Neubert[75], N. Neufeld[48], R. Newcombe[61], T. D. Nguyen[49], C. Nguyen-Mau[49,w], E. M. Niel[11], S. Nieswand[14], N. Nikitin[40], N. S. Nolte[48], C. Nunez[85], A. Oblakowska-Mucha[34], V. Obraztsov[44], D. P. O'Hanlon[54], R. Oldeman[27,d], M. E. Olivares[68], C. J. G. Onderwater[78], A. Ossowska[35], J. M. Otalora Goicochea[2], T. Ovsiannikova[41], P. Owen[50], A. Oyanguren[47], B. Pagare[56], P. R. Pais[48], T. Pajero[29,l,48], A. Palano[19], M. Palutan[23], Y. Pan[62], G. Panshin[83], A. Papanestis[57], M. Pappagallo[19,b], L. L. Pappalardo[21,e], C. Pappenheimer[65], W. Parker[66], C. Parkes[62], C. J. Parkinson[46], B. Passalacqua[21], G. Passaleva[22], A. Pastore[19], M. Patel[61], C. Patrignani[20,c], C. J. Pawley[79], A. Pearce[48], A. Pellegrino[32], M. Pepe Altarelli[48], S. Perazzini[20], D. Pereima[41], P. Perret[9], K. Petridis[54], A. Petrolini[24,g], A. Petrov[80], S. Petrucci[58], M. Petruzzo[25], A. Philippov[42], L. Pica[29], M. Piccini[77], B. Pietrzyk[8], G. Pietrzyk[49], M. Pili[63], D. Pinci[30], F. Pisani[48], A. Piucci[17], Resmi P.K[10], V. Placinta[37], J. Plews[53], M. Plo Casasus[46], F. Polci[13], M. Poli Lener[23], M. Poliakova[68], A. Poluektov[10], N. Polukhina[82,t], I. Polyakov[68], E. Polycarpo[2], G. J. Pomery[54], S. Ponce[48], D. Popov[6,48], S. Popov[42], S. Poslavskii[44], K. Prasanth[35], L. Promberger[48], C. Prouve[46], V. Pugatch[52], H. Pullen[63], G. Punzi[29,m], W. Qian[6], J. Qin[6], R. Quagliani[13], B. Quintana[8], N. V. Raab[18], R. I. Rabadan Trejo[10], B. Rachwal[34], J. H. Rademacker[54], M. Rama[29], M. Ramos Pernas[56], M. S. Rangel[2], F. Ratnikov[42,81], G. Raven[33], M. Reboud[8], F. Redi[49], F. Reiss[13], C. Remon Alepuz[47], Z. Ren[3], V. Renaudin[63], R. Ribatti[29], S. Ricciardi[57], D. S. Richards[57], K. Rinnert[60], P. Robbe[11], A. Robert[13], G. Robertson[58], A. B. Rodrigues[49], E. Rodrigues[60], J. A. Rodriguez Lopez[74], A. Rollings[63], P. Roloff[48], V. Romanovskiy[44], M. Romero Lamas[46], A. Romero Vidal[46], J. D. Roth[85], M. Rotondo[23], M. S. Rudolph[68], T. Ruf[48], J. Ruiz Vidal[47], A. Ryzhikov[81], J. Ryzka[34], J. J. Saborido Silva[46], N. Sagidova[38], N. Sahoo[56], B. Saitta[27,d], D. Sanchez Gonzalo[45], C. Sanchez Gras[32], R. Santacesaria[30], C. Santamarina Rios[46], M. Santimaria[23], E. Santovetti[31,o], D. Saranin[82], G. Sarpis[59], M. Sarpis[75], A. Sarti[30], C. Satriano[30,n], A. Satta[31], M. Saur[15], D. Savrina[40,41], H. Sazak[9], L. G. Scantlebury Smead[63], S. Schael[14], M. Schellenberg[15], M. Schiller[59], H. Schindler[48], M. Schmelling[16], B. Schmidt[48], O. Schneider[49], A. Schopper[48], M. Schubiger[32], S. Schulte[49], M. H. Schune[11], R. Schwemmer[48], B. Sciascia[23], A. Sciubba[23], S. Sellam[46], A. Semennikov[41], M. Senghi Soares[33], A. Sergi[48,53], N. Serra[50], L. Sestini[28], A. Seuthe[15], P. Seyfert[48], D. M. Shangase[85], M. Shapkin[44], I. Shchemerov[82], L. Shchutska[49], T. Shears[60], L. Shekhtman[43,u], Z. Shen[5], V. Shevchenko[80], E. B. Shields[26,i], E. Shmanin[82], J. D. Shupperd[68], B. G. Siddi[21], R. Silva Coutinho[50], G. Simi[28], S. Simone[19,b], I. Skiba[21,e], N. Skidmore[62], T. Skwarnicki[68], M. W. Slater[53], J. C. Smallwood[63], J. G. Smeaton[55],

A. Smetkina[41], E. Smith[14], M. Smith[61], A. Snoch[32], M. Soares[20], L. Soares Lavra[9], M. D. Sokoloff[65], F. J. P. Soler[59], A. Solovev[38], I. Solovyev[38], F. L. Souza De Almeida[2], B. Souza De Paula[2], B. Spaan[15], E. Spadaro Norella[25,h], P. Spradlin[59], F. Stagni[48], M. Stahl[65], S. Stahl[48], P. Stefko[49], O. Steinkamp[50,82], S. Stemmle[17], O. Stenyakin[44], H. Stevens[15], S. Stone[68], M. E. Stramaglia[49], M. Straticiuc[37], D. Strekalina[82], S. Strokov[83], F. Suljik[63], J. Sun[27], L. Sun[73], Y. Sun[66], P. Svihra[62], P. N. Swallow[53], K. Swientek[34], A. Szabelski[36], T. Szumlak[34], M. Szymanski[48], S. Taneja[62], F. Teubert[48], E. Thomas[48], K. A. Thomson[60], M. J. Tilley[61], V. Tisserand[9], S. T'Jampens[8], M. Tobin[4], S. Tolk[48], L. Tomassetti[21,e], D. Torres Machado[1], D. Y. Tou[13], M. Traill[59], M. T. Tran[49], E. Trifonova[82], C. Trippl[49], G. Tuci[29,m], A. Tully[49], N. Tuning[32], A. Ukleja[36], D. J. Unverzagt[17], A. Usachov[32], A. Ustyuzhanin[42,81], U. Uwer[17], A. Vagner[83], V. Vagnoni[20], A. Valassi[48], G. Valenti[20], N. Valls Canudas[45], M. van Beuzekom[32], E. van Herwijnen[82], C. B. Van Hulse[18], M. van Veghel[78], R. Vazquez Gomez[46], P. Vazquez Regueiro[46], C. Vázquez Sierra[48], S. Vecchi[21], J. J. Velthuis[54], M. Veltri[22,q], A. Venkateswaran[68], M. Veronesi[32], M. Vesterinen[56], D. Vieira[65], M. Vieites Diaz[49], H. Viemann[76], X. Vilasis-Cardona[84], E. Vilella Figueras[60], P. Vincent[13], G. Vitali[29], A. Vollhardt[50], D. Vom Bruch[13], A. Vorobyev[38], V. Vorobyev[43,u], N. Voropaev[38], R. Waldi[76], J. Walsh[29], C. Wang[17], J. Wang[73], J. Wang[3], J. Wang[5], J. Wang[4], M. Wang[3], R. Wang[54], Y. Wang[7], Z. Wang[50], H. M. Wark[60], N. K. Watson[53], S. G. Weber[13], D. Websdale[61], C. Weisser[64], B. D. C. Westhenry[54], D. J. White[62], M. Whitehead[54], D. Wiedner[15], G. Wilkinson[63], M. Wilkinson[68], I. Williams[55], M. Williams[64,69], M. R. J. Williams[58], F. F. Wilson[57], W. Wislicki[36], M. Witek[35], L. Witola[17], G. Wormser[11], S. A. Wotton[55], H. Wu[68], K. Wyllie[48], Z. Xiang[6], D. Xiao[7], Y. Xie[7], A. Xu[5], J. Xu[6], L. Xu[3], M. Xu[7], Q. Xu[6], Z. Xu[6], Z. Xu[5], D. Yang[3], Y. Yang[6], Z. Yang[3], Z. Yang[66], Y. Yao[68], L. E. Yeomans[60], H. Yin[7], J. Yu[71], X. Yuan[68], O. Yushchenko[44], K. A. Zarebski[53], M. Zavertyaev[16,t], M. Zdybal[35], O. Zenaiev[48], M. Zeng[3], D. Zhang[7], L. Zhang[3], S. Zhang[5], Y. Zhang[5], Y. Zhang[63], A. Zhelezov[17], Y. Zheng[6], X. Zhou[6], Y. Zhou[6], X. Zhu[3], V. Zhukov[14,40], J. B. Zonneveld[58], S. Zucchelli[20,c], D. Zuliani[28], G. Zunica[62]

1 Centro Brasileiro de Pesquisas Físicas (CBPF), Rio de Janeiro, Brazil
2 Universidade Federal do Rio de Janeiro (UFRJ), Rio de Janeiro, Brazil
3 Center for High Energy Physics, Tsinghua University, Beijing, China
4 Institute Of High Energy Physics (IHEP), Beijing, China
5 School of Physics State Key Laboratory of Nuclear Physics and Technology, Peking University, Beijing, China
6 University of Chinese Academy of Sciences, Beijing, China
7 Institute of Particle Physics, Central China Normal University, Wuhan, Hubei, China
8 Univ. Grenoble Alpes, Univ. Savoie Mont Blanc, CNRS, IN2P3-LAPP, Annecy, France
9 Université Clermont Auvergne, CNRS/IN2P3, LPC, Clermont-Ferrand, France
10 Aix Marseille Univ, CNRS/IN2P3, CPPM, Marseille, France
11 Université Paris-Saclay, CNRS/IN2P3, IJCLab, Orsay, France
12 Laboratoire Leprince-ringuet (llr), Palaiseau, France
13 LPNHE, Sorbonne Université, Paris Diderot Sorbonne Paris Cité, CNRS/IN2P3, Paris, France
14 I. Physikalisches Institut, RWTH Aachen University, Aachen, Germany
15 Fakultät Physik, Technische Universität Dortmund, Dortmund, Germany
16 Max-Planck-Institut für Kernphysik (MPIK), Heidelberg, Germany
17 Physikalisches Institut, Ruprecht-Karls-Universität Heidelberg, Heidelberg, Germany
18 School of Physics, University College Dublin, Dublin, Ireland
19 INFN Sezione di Bari, Bari, Italy
20 INFN Sezione di Bologna, Bologna, Italy
21 INFN Sezione di Ferrara, Ferrara, Italy
22 INFN Sezione di Firenze, Firenze, Italy
23 INFN Laboratori Nazionali di Frascati, Frascati, Italy
24 INFN Sezione di Genova, Genova, Italy
25 INFN Sezione di Milano, Milano, Italy
26 INFN Sezione di Milano-Bicocca, Milano, Italy
27 INFN Sezione di Cagliari, Monserrato, Italy
28 Universita degli Studi di Padova, Universita e INFN, Padova, Padova, Italy
29 INFN Sezione di Pisa, Pisa, Italy
30 INFN Sezione di Roma La Sapienza, Roma, Italy
31 INFN Sezione di Roma Tor Vergata, Roma, Italy

[32] Nikhef National Institute for Subatomic Physics, Amsterdam, Netherlands

[33] Nikhef National Institute for Subatomic Physics and VU University Amsterdam, Amsterdam, Netherlands

[34] AGH - University of Science and Technology, Faculty of Physics and Applied Computer Science, Kraków, Poland

[35] Henryk Niewodniczanski Institute of Nuclear Physics Polish Academy of Sciences, Kraków, Poland

[36] National Center for Nuclear Research (NCBJ), Warsaw, Poland

[37] Horia Hulubei National Institute of Physics and Nuclear Engineering, Bucharest-Magurele, Romania

[38] Petersburg Nuclear Physics Institute NRC Kurchatov Institute (PNPI NRC KI), Gatchina, Russia

[39] Institute for Nuclear Research of the Russian Academy of Sciences (INR RAS), Moscow, Russia

[40] Institute of Nuclear Physics, Moscow State University (SINP MSU), Moscow, Russia

[41] Institute of Theoretical and Experimental Physics NRC Kurchatov Institute (ITEP NRC KI), Moscow, Russia

[42] Yandex School of Data Analysis, Moscow, Russia

[43] Budker Institute of Nuclear Physics (SB RAS), Novosibirsk, Russia

[44] Institute for High Energy Physics NRC Kurchatov Institute (IHEP NRC KI), Protvino, Russia, Protvino, Russia

[45] ICCUB, Universitat de Barcelona, Barcelona, Spain

[46] Instituto Galego de Física de Altas Enerxías (IGFAE), Universidade de Santiago de Compostela, Santiago de Compostela, Spain

[47] Instituto de Fisica Corpuscular, Centro Mixto Universidad de Valencia - CSIC, Valencia, Spain

[48] European Organization for Nuclear Research (CERN), Geneva, Switzerland

[49] Institute of Physics, Ecole Polytechnique Fédérale de Lausanne (EPFL), Lausanne, Switzerland

[50] Physik-Institut, Universität Zürich, Zürich, Switzerland

[51] NSC Kharkiv Institute of Physics and Technology (NSC KIPT), Kharkiv, Ukraine

[52] Institute for Nuclear Research of the National Academy of Sciences (KINR), Kyiv, Ukraine

[53] University of Birmingham, Birmingham, UK

[54] H.H. Wills Physics Laboratory, University of Bristol, Bristol, UK

[55] Cavendish Laboratory, University of Cambridge, Cambridge, UK

[56] Department of Physics, University of Warwick, Coventry, UK

[57] STFC Rutherford Appleton Laboratory, Didcot, UK

[58] School of Physics and Astronomy, University of Edinburgh, Edinburgh, UK

[59] School of Physics and Astronomy, University of Glasgow, Glasgow, UK

[60] Oliver Lodge Laboratory, University of Liverpool, Liverpool, UK

[61] Imperial College London, London, UK

[62] Department of Physics and Astronomy, University of Manchester, Manchester, UK

[63] Department of Physics, University of Oxford, Oxford, UK

[64] Massachusetts Institute of Technology, Cambridge, MA, USA

[65] University of Cincinnati, Cincinnati, OH, USA

[66] University of Maryland, College Park, MD, USA

[67] Los Alamos National Laboratory (LANL), Los Alamos, USA

[68] Syracuse University, Syracuse, NY, USA

[69] School of Physics and Astronomy, Monash University, Melbourne, Australia

[70] Pontifícia Universidade Católica do Rio de Janeiro (PUC-Rio), Rio de Janeiro, Brazil

[71] Physics and Micro Electronic College, Hunan University, Changsha City, China

[72] Guangdong Provencial Key Laboratory of Nuclear Science, Institute of Quantum Matter, South China Normal University, Guangzhou, China

[73] School of Physics and Technology, Wuhan University, Wuhan, China

[74] Departamento de Fisica , Universidad Nacional de Colombia, Bogota, Colombia

[75] Universität Bonn-Helmholtz-Institut für Strahlen und Kernphysik, Bonn, Germany

[76] Institut für Physik, Universität Rostock, Rostock, Germany

[77] INFN Sezione di Perugia, Perugia, Italy

[78] Van Swinderen Institute, University of Groningen, Groningen, Netherlands

[79] Universiteit Maastricht, Maastricht, Netherlands

[80] National Research Centre Kurchatov Institute, Moscow, Russia

[81] National Research University Higher School of Economics, Moscow, Russia

[82] National University of Science and Technology "MISIS", Moscow, Russia

[83] National Research Tomsk Polytechnic University, Tomsk, Russia

[84] DS4DS, La Salle, Universitat Ramon Llull, Barcelona, Spain

[85] University of Michigan, Ann Arbor, USA

[a] Universidade Federal do Triângulo Mineiro (UFTM), Uberaba-MG, Brazil

[b] Università di Bari, Bari, Italy

[c] Università di Bologna, Bologna, Italy

[d] Università di Cagliari, Cagliari, Italy

[e] Università di Ferrara, Ferrara, Italy

[f] Università di Firenze, Firenze, Italy

[g] Università di Genova, Genova, Italy

[h] Università degli Studi di Milano, Milano, Italy

[i] Università di Milano Bicocca, Milano, Italy

[j] Università di Modena e Reggio Emilia, Modena, Italy

[k] Università di Padova, Padova, Italy

[l] Scuola Normale Superiore, Pisa, Italy

[m] Università di Pisa, Pisa, Italy

[n] Università della Basilicata, Potenza, Italy

[o] Università di Roma Tor Vergata, Roma, Italy

[p] Università di Siena, Siena, Italy

[q] Università di Urbino, Urbino, Italy

[r] MSU - Iligan Institute of Technology (MSU-IIT), Iligan, Philippines

[s] AGH - University of Science and Technology, Faculty of Computer Science, Electronics and Telecommunications, Kraków, Poland

[t] P.N. Lebedev Physical Institute, Russian Academy of Science (LPI RAS), Moscow, Russia

[u] Novosibirsk State University, Novosibirsk, Russia

[v] Department of Physics and Astronomy, Uppsala University, Uppsala, Sweden

[w] Hanoi University of Science, Hanoi, Vietnam